Robust and Highly Efficient Extractions of Proteins from Bones enable Deep, High-Throughput Proteomic Quantification to Gain Insights into Bone Biology

Jacob P. Rose[1], Charles A. Schurman[1], Christina D. King[1], Joanna Bons[1], Jordan B. Burton[1], Sandip K. Patel[1], Amy O'Broin[1], Tamara Alliston [2], Birgit Schilling[1*]

[1] Buck Institute for Research on Aging, Novato, CA, USA

[2] University of California, San Francisco, Department of Orthopaedic Surgery, San Francisco, CA, USA

* Corresponding author: Birgit Schilling

Email: bschilling@buckinstitute.org

Short title: Novel Efficient Bone Proteomic Workflows

Abstract

Dysregulation of cell signaling in bone cells, such as osteocytes, osteoblasts, osteoclasts, and chondrocytes, and elevated burden of senescent cells in bone and cartilage, are implicated in osteoarthritis (OA). Mass spectrometric analyses provides a crucial molecular tool-kit to understand complex signaling relationships in age-related diseases, such as OA. Here we introduce a novel mass spectrometric workflow to promote proteomic studies of bone and cartilage. This workflow uses highly specialized steps, including extensive overnight demineralization, pulverization, and incubation for 72 h in 6 M guanidine hydrochloride and EDTA, followed by proteolytic digestion. Analysis on a high-resolution Orbitrap Eclipse and Orbitrap Exploris 480 mass spectrometer using Data-Independent Acquisition (DIA) provides deep coverage of the bone proteome, and preserves post-translational modifications, such as hydroxyproline. A spectral library-free quantification strategy, directDIA, identified and quantified over 2,000 protein groups (with ≥ 2 unique peptides) from calcium-rich bone matrices. Key components identified were proteins of the extracellular matrix (ECM), bone-specific proteins (e.g., bone sialoprotein 2, IBSP), and signaling proteins (e.g., transforming growth factor beta-2, TGFB2) and lysyl oxidase homolog 2 (LOXL2), an important protein in collagen crosslinking. Post-translational modifications (PTMs) were identified without the need for specific enrichment. This includes collagen hydroxyproline modifications, chemical modifications for collagen self-assembly and network formation. Multiple senescence factors were identified, such as C3 protein of the complement system and many matrix metalloproteinases, that might be monitored during age-related bone disease progression. Our innovative workflow yields in-depth protein coverage and quantification strategies to discover underlying biological mechanisms of bone aging and to provide tools to monitor therapeutic interventions.

Introduction

Age-related bone fragility typically results from the decline of both bone mass and bone quality over the lifetime of an organism (1, 2) and leads to bone and joint diseases, such as osteoporosis and osteoarthritis (OA). As these pathologies are tightly correlated with increasing age, their impact is more drastic in aging populations, and case rates are rising worldwide as individual lifespans increase. Indeed, global OA case rates have risen by about 10% between 1990 and 2017, and case rates in the United States of America have increased by 23% in that same time. Currently, OA prevalence in the USA is over 6,000 cases per 100,000 people as reported in 2020 (3). Unfortunately, the link between OA or osteoporosis and aging and neurodegeneration (4), is poorly understood, despite clinical and molecular evidence for their relationship (4-6). Clinically relevant assays and biomarkers are crucially needed to diversify treatment options and to monitor treatment efficacy.

Skeletal biology is a complex and multi-faceted ecosystem of cell types, including bone-building osteoblasts and bone-resorbing osteoclasts. Most importantly, the bone matrix is supported and nourished by osteocytes embedded within the calcified structure of the bone, and chondrocytes reside within and maintain articular cartilage. Osteocytes represent 90–95% of all cell types within the bone, and signal and communicate directly via dendritic processes and through secretion of proteins that can influence the formation and activity of osteoblasts and osteoclasts. Aging and increased cellular senescence burden impact all cell types within bone, alter their natural function, and lead to tissue degeneration (**Figure 1)** (2, 7, 8).

With age, the balance between osteoblast regulated bone deposition and osteoclast mediated bone resorption is disrupted: bone resorption begins to outpace bone deposition, leading to lost bone mass (2, 9). Osteocyte dendritic processes typically decrease significantly with age (10), and other mechanisms that maintain bone tissue material properties decline (11, 12). Thus, aging in the skeleton is associated with both osteopenia and osteoporosis, clinical conditions of low bone mass, that lead to increased rates of fracture in aged-populations and fragility fractures in individuals with clinically normal bone mass (13, 14). Additionally, joint disease progression, such as OA, is associated with advancing age as the cellular and material regulatory mechanisms maintaining cartilage decline (15, 16). Temporal alterations to skeletal

cell behavior, including a shift of homeostatic mechanisms towards more inflammatory phenotypes, also contribute to the breakdown of skeletal tissues and lead to age-related diseases.

One cellular mechanism associated with both inflammation and aging is cellular senescence. During senescence, homeostatic cells exit their normal cell cycles and adopt a senescence-associated secretory phenotype (SASP) that is characterized by a host of inflammatory secreted factors (17-19). The role that the SASP and senescence play in bone health is well documented (20, 21), but also understudied on a molecular level. Recent efforts examined biomarkers of senescence and senescence burden in multiple disease pathologies, including OA (22, 23). Skeletal tissue is especially susceptible to damage via the SASP as secreted factors may not only alter skeletal cell behavior but directly damage skeletal tissues that enable locomotion (20, 24). While the SASP contains a broad range of factors, several of the most well identified markers include matrix metalloproteinases, other proteolytic enzymes, and ATPase ion pumps that regulate intracellular and pericellular pH (18, 25). These factors are normally well regulated by skeletal cells, and are used to maintain tissue quality, but with age their unchecked action can directly damage skeletal tissues leading to age-related skeletal disease. In addition, many of the intricate and well-regulated molecular signaling pathways that maintain balanced bone deposition and resorption can be members of, or targeted by, SASP. For instance, both sclerostin (SOST) and receptor activator of NF-κβ ligand (RANKL) are secreted proteins produced by osteocytes that increase in serum with age. These factors are linked to senescence within bone cells and directly shift bone remodeling towards bone resorption by suppressing osteoblast bone formation and increasing osteoclastic bone resorption, respectively (26-30). Dysregulation of signaling in skeletal cells and an elevated senescent burden are implicated in bone aging and in progressive loss of mechanical function that leads to bone frailty, osteoporosis, and osteoarthritis (1, 31). With the important roles of secreted proteins in both skeletal tissue remodeling and managing skeletal cell type function, along with their altered behavior in age and senescence, there is a dire need to develop molecular tools that directly measure protein presence and quantitative regulation in the context of age-related skeletal diseases.

Large-scale unbiased analytical techniques, such as transcriptomics, proteomics, metabolomics, and lipidomics, are powerful methods that are often used to gain comprehensive insights into complex biological systems and their changes in aging and diseases. Several successful transcriptomics and single-cell-sequencing efforts have been undertaken in bones (32-34), but few quantitative bone proteomic studies have been published (35-40). Given the structural relevance of extracellular matrix (ECM) proteins and signaling peptides within the skeleton, analyzing bone proteome profiles during aging and age-related skeletal biology will be highly beneficial and insightful. Proteomic studies appear to be limited in skeletal tissues, possibly due to the complex, dense and mineralized matrix, and overall analytical challenges of efficient protein extraction using existing protocols. The mineralized ECM of bone contains large amounts of calcium in the form of matrix-bound hydroxyapatite, $Ca_{10}(PO_4)_6(OH)_2$, that is embedded within and around collagen fibrils. These hydroxyapatite minerals cause nonspecific interactions between positively charged amino acids with phosphate groups and carboxyl residue complexes with calcium (41), and thus, conventional protein lysis extractions often fail or are inefficient. Protein extraction techniques that disrupt nonspecific interactions and carboxyl residue complexes between proteins and hydroxyapatite are critically needed for efficient and comprehensive protein coverage in bone.

The protein compositions within bone and other skeletal tissues are highly specialized in form and function. Uniquely, post-translation modifications of individual pro-collagen molecules through proline oxidation are required to stabilize the triple-helix structure of collagen itself through stereo-electric effects or water-bridged hydrogen bonding (42). Genetic disorders, such as osteogenesis imperfecta (43) and others that interrupt hydroxyproline modifications are phenotypically characterized by brittle bones in young patients (44) and resemble some age-related pathologies. Capturing post-translational modifications (PTMs) and their interactions among structural proteins within the skeleton is critical for assessing bone health, and proteomic methods that preserve these alterations are crucial for studying skeletal tissues.

With this study, we present a novel proteomic workflow to globally study osteoarthritis, osteoporosis, and other age-related skeletal pathologies by examining the changes within the proteomic landscape between bone and cartilage. Deep protein coverage and quantification are

achieved with our novel robust and reproducible proteomics protocol to efficiently extract proteins from the complex bone matrix and the subsequent combination with modern quantitative mass spectrometric strategies. We adapted and improved steps from a reported method that extracted proteins from bones (45), as well as from cystinuric bladder stones (46). When paired with data-independent acquisition (DIA) mass spectrometry (MS) (47-49), this novel workflow profiles and quantifies both dynamic changes in protein composition, as well as PTM signaling to investigate bone aging and diseases. The application of quantitative proteomics to further understand bone cell signaling dynamics in the context of aging and cellular senescence is expected to lead to the discovery of novel biomarkers and to discover new therapeutic targets for the treatments of age-related bone diseases.

Results

Reproducible protein extraction from mouse bones and proteomic analysis

Our novel workflow comprises highly-specialized steps, including collection of femur bones from C57/BL6 mice, removing and flushing the bone marrow, followed by extensive demineralization overnight, pulverization, incubation for 72 h in 6 M guanidine hydrochloride and EDTA to extract proteins, a buffer exchange to remove the guanidine hydrochloride and, finally, proteolytic digestion of the extracted protein lysates (see **Figure 2**). Protein concentrations were initially determined with a bicinchoninic acid assay, as a first step of quality control and to demonstrate successful protein extraction. Subsequently, bone protein lysates were prepared for LC–MS/MS analysis. Pooled samples from four bone groups were proteolytically digested with trypsin, and peptides were analyzed on an Orbitrap Exploris 480 and an Orbitrap Eclipse Tribrid (Thermo). Briefly, we used a label-free, highly quantitative DIA-MS approach, in which the sequential selection of MS1 precursor ion windows (or m/z segments) for MS/MS enable that the entire MS1 mass range was subjected to fragmentation within each scan cycle throughout the entire gradient (47, 49). This comprehensive acquisition utilized a precursor ion isolation scheme that consisted of 26 variable windows and covered an *m/z* range of 350–1,650 with an overlap of 1 *m/z* per each DIA window (50). Data files were processed using a spectral library-free strategy, referred to as directDIA within the Spectronaut algorithm (Biognosys) (51, 52).

Acquisitions were assessed for quality control by displaying their retention time regressions plotting the indexed retention time in relation to the observed retention time with a representative graph shown in **Figure 3a**. Each point along the curve represents a measured precursor ion and its retention regression. These indexed retention time regressions were normalized for slight variations in measured retention times from acquisition to acquisition, and thus improve the quantification accuracy. DIA-MS acquisitions assayed reproducibility by measuring coefficients of variation (CV). **Figure 3b** visualizes the precursor ion CV distribution correlating the precursor ion CV values against the respective measured peak area abundances and indicating very high reproducibility. As expected, very low abundant analytes appear to be more variable. However, across five MS replicates, a median CV of 8.7% was reported for precursor ions, and 85% of precursor ions featured a CV that was smaller than 20% (**Figure 3c-d and Supplemental Table S1**).

In-depth Coverage of Extracellular Matrix (ECM) Proteins from Mouse Femurs

In a separate study, we next assessed observed protein pathways and deep protein coverage within mouse femoral bones. A cohort of five C57/B6J wild-type (WT) mice was utilized to isolate femurs, followed by our optimized workflow for protein extraction and proteolytic digestion. Mass spectrometric DIA analysis of the digested protein lysates on an Orbitrap Eclipse (Thermo) from this independent cohort of mice resulted in the confident identification and quantification of 2,108 protein groups, identified with ≥2 unique peptides **(Supplemental Table S2 Excel)**.

We performed various Gene Ontology (GO) analyses to determine which cellular compartments and biological processes were enriched in this bone-derived protein dataset. GO cellular compartments, such as the cytoplasm, nucleus, plasma membrane, and the extracellular region, presented most of the annotated identifications and showed that a variety of proteins were included in this proteome analysis (**Figure 4a)**. In addition, a biological process GO analysis showed broad enrichment for diverse cellular processes: both intercellular and extracellular processes (e.g., oxidative phosphorylation, tricarboxylic acid cycle, and collagen metabolic processes) and mechanical processes (e.g., collagen fibril organization, collagen catabolism, endochondral bone growth, and musculoskeletal movement) as shown in **Figure 4b and**

Supplemental Table S3. These results highlight a major strength of the sample preparation process, because capturing diverse protein profiles that include highly abundant ECM components, such as collagens and proteoglycans, and metabolic or signaling proteins, such as TGF beta, is incredibly valuable to bone biology. To more completely interrogate bone-specific proteins, we assessed protein coverage and peak quality for secreted protein acidic and cysteine rich (SPARC), a protein typically secreted by osteoblasts during bone formation (53).

Detection of Functionally Diverse Collagens and Formation of Structural Networks

We next examined the coverage of collagens identified using this novel bone proteomics methodology. Collagens are a diverse family of proteins that are important for bone biology (54). Robust analytical assays that detect most collagens, efficiently monitor, and accurately quantify them are important for the study of bone or cartilage (55). In our analysis, we identified major functional types of collagens, including a majority of fibrillar collagens (e.g., collagens type I, II, III, and V) and multiple chains of collagen IV, which forms beaded filament assemblies. Additionally, we confidently identified multiple "fibril-associated collagens with interrupted triple helices" (FACITs), including collagen types IX, XII, XIV, XVI, and XXII. Over 75% of the identified collagens belonged to the fibrillar functional family with the largest majority (48%) being Collagen type I **(Figure 5)**. The second most abundant functional family identified was the FACIT family (~10% of total collagens), interestingly we identified multiple members of the thrombospondin family (Thbs1-4), including Thbs1 which is the major protein involved in structural assembly and FACIT biology (56).

Preservation of Hydroxyproline Modifications

PTMs are biologically relevant for many tissue types (57). In bone, we analyzed hydroxyproline modifications, including the determination of proline PTM site-localization within the measured peptides and proteins. Hydroxyproline is an important PTM, specifically in collagens, that helps stabilize 3-dimensional protein-protein interactions among different collagen chains (42, 54). To confidently identify and site-localize hydroxyproline modifications (+ 15.99 Da), we initially processed our samples using data-dependent acquisition (DDA), where precursor ions are

isolated in 'tight' windows (1 m/z), and are then subjected to MS/MS, providing less complex and highly specific MS/MS spectra. To generate true quantitative assays and to query these modifications using quantitative DIA acquisitions, we generated a spectral library that included the 1,382 DDA-identified hydroxyproline-containing peptides using Spectronaut. Importantly, we determined that hydroxyproline modifications are not significantly degraded in our sample preparation and can be subjected to these new quantitative assays generated. This search resulted in 1,186 hydroxyproline modified peptides with 85% site probability, corresponding to 75 modified proteins **(Supplemental Table S4B)**. In fact, our novel MS workflow allowed the identification of a hydroxyproline modified residue Pro-707 (in bold below), a previously reported (58), structurally relevant site on collagen alpha-1(I) chain. The modified peptide is shown (GDTGAPoxGA**Pox**GSQGAPoxGLQGMPoxGER, Col1a1), featuring both the MS/MS and the extracted ion chromatogram (XIC) **(Figure 6a).** In this example we confirmed the presence of 4 hydroxyproline residues with direct and indirect ion evidence including the y_4, y_5, y_{10}, y_{16}, and y_{19} ions. In addition, we determined that Pro-533 (GLTGS**Pox**GSPGPDGK, Col1a1) was modified and displayed a nearly complete fragment ion series that provided accurate mapping of the hydroxy modification using differentiating ions like y_4, y_6, and y_9 **(Figure 6b)**. These results exhibit the power of this analysis to confidently capture and localize biologically relevant PTMs with no prior sample enrichment that is commonly required for PTM studies.

Quantification of biologically relevant ECM components and senescence markers

This dataset was initially compared to the core matrisome published by Naba et al. (59-61) to determine the level of coverage, compared to this rich proteomic dataset. We found that 42% of bone proteins overlapped with the known murine core matrisome (**Supplemental Table S5a**), suggesting that extracted bone proteins are largely composed of ECM and ECM-related proteins. Specifically, our dataset was compared to each component of the core matrisome, such as glycoproteins, collagens, proteoglycans, ECM affiliated proteins, ECM regulator proteins, and secreted proteins **(Figure 7a)**. Specifically, we identified 70 glycoproteins and 71 ECM regulators that are part of the core matrisome. In addition to the matrisome data base, we analyzed our results in reference to a proteomic analysis of the Senescence Associated Secretory Phenotype

(SASP) published by Basisty et al. (18). In the latter publication our group outlined commonly identified proteins in the SASP using multiple inducers of senescence, considering them the Core SASP. The results from this comparison showed that 131 Core SASP factors are identified in this analysis. These common identifications include ECM organizing proteins, such as matrix metalloproteinases (MMP2), lysyl oxidase-like 2, biglycan, TIMP metallopeptidase inhibitor 2 (TIMP2), and serpin H1. Additionally, insulin signaling proteins, including multiple insulin-like growth factors, and certain members of the immune system, such as macrophage migration inhibitory factor (MIF) and high mobility group box 1 (HMGB1), were identified **(Figure 7b)**. Indeed, many of the Core SASP proteins have been quantified here, and the comparisons presented described the relevance and depth of this proteomic workflow.

Discussion

A novel demineralization and extraction protocol was developed to obtain deep proteomic profiles for bones to study age-related bone conditions, such as OA. Proteins were extracted and digested, and proteolytic peptides were analyzed using DIA-MS for identification and quantification of relevant molecular signatures in bone. Many bone-specific proteins and proteins important to skeletal biology were identified, including important ECM proteins, collagen-specific PTMs that influence collagen structural assembly, and potential senescence/SASP factors. Additionally, proteins identifying specific bone cell types, such as osteopontin/bone sialoprotein 1 (Opn/Bsp-1) for osteoblasts, matrix extracellular phosphoglycoprotein (Mepe) for osteocytes, and tartrate-resistant acid phosphatase type 5(TRAP) for osteoclasts, were found and confirmed bone cellular identity in our analysis.

This proteomic protocol was optimized to overcome challenges in the bone matrix that interfere with accurate protein identification and quantification. The initial demineralization step was crucial and greatly helped to preprocess the lysates by removing calcium phosphate deposits while leaving ECM proteins intact in the organic matrix that remained. The other protocol steps were designed to provide an extremely efficient and reproducible workflow using S-trap columns for purification and digestion of the samples and HLB cartridges for desalting of the proteolytic peptides.

The samples were then acquired in DIA mode and processed using directDIA (Spectronaut). Searching the acquisitions in this spectral library-free fashion saves sample amounts and instrument acquisition time. This resulted in a comprehensive bone proteome profile featuring tissue-specific, and potentially disease-relevant protein candidates. To enhance our study at the post-translational level, we investigated bone samples with DDA, and identifed PTM-containing proteolytic peptides. Subsequently we built custom PTM spectral libraries and were able to use these to extract hydroxyproline containing peptides from our DIA data, especially focusing on collagen I. Additionally, senescence markers relevant to OA progression, such as matrix altering proteins, such as metalloproteinase 2 (MMP2), metalloproteinase inhibitors 1 and 2 (TIMP1 and 2, and signaling proteins, were also identified. Identification of well-characterized SASP factors, including HMGB1, illustrated the potential to use proteomics to assay bone senescence. Indeed, the effects of cellular senescence in other related tissues, such as cartilage, have been implicated but not characterized with rigorous proteomics, especially after proposed treatments for OA, senolytics, or other cartilage rejuvenation therapeutics. The ECM greatly influences cell signaling and cell function and is a significant determinant of cell fate by sensing mechanical stimuli from the stroma (62-64).

We presented that the bone, as a tissue, is robustly composed of ECM and therefore changes in the ECM will be at the forefront of its biology. These results will provide insight to other tissues where the ECM or mechano-sensing pathways could be more important than previously described, such as in the muscle, cartilage, breast, and ovary. Proteomics studies are uniquely positioned to capture relevant information about collagen ratios, senescence markers, and disease contributors in the bone microenvironment using a highly confident and quantitative mass spectrometric analysis.

This new integrated proteomic workflow combining the thorough bone protein extraction protocol with a comprehensive DIA-MS analysis will allow us to analyze human and other mammalian bone samples, specifically in the context of osteoarthritis. We will be able to dynamically monitor disease progression, and potentially discover new biomarkers and provide tools to monitor therapeutic interventions.

Materials and Methods

Reagents and Standards. HPLC solvents (e.g., acetonitrile and water) were obtained from Burdick & Jackson (Muskegon, MI). Reagents for protein chemistry (e.g., iodoacetamide, dithiothreitol, guanidine hydrochloride, EDTA, and formic acid) were purchased from Sigma Aldrich (St. Louis, MO). Proteomics grade trypsin was from Promega (Madison WI). HLB Oasis SPE cartridges were purchased from Waters (Milford, MA).

Protein Extraction from Bones. The long bones from C57/B6J (WT) mice at age 16 weeks were stripped of any muscle or cartilage, and the marrow was removed to reduce sample complexity. Bones were demineralized overnight by adding 1 mL of 1.2 M HCl and rotating them overnight at 4 °C (45).The demineralized bones were subsequently transferred to a new Eppendorf tube and kept on dry ice until pulverization. All components of the homogenizer, including sample tubes and homogenizing plates, were cooled with liquid nitrogen. Frozen bones were subsequently pulverized with the SPEX SamplePrep 1600 MiniG tissue homogenizer in polycarbonate tubes with a 9.5-mm steel grinding ball for 2 minutes at 1500 strokes/minute. After the first 2 minutes, the samples were removed from the homogenizer, allowed to cool in liquid nitrogen for 3 minutes, and homogenized for another 2 minutes at 1500 strokes/minute. Pulverized samples were transferred into a fresh Eppendorf tube using 800 µL of extraction buffer (6 M guanidine hydrochloride, 10 mM Tris-HCl, 50 mM EDTA) and incubated by rotating at 4 °C for 72 hours (65). Subsequently, the samples were spun for 3 minutes at 15,000 x *g* to separate bone matrix and the supernatants. Supernatants containing the soluble proteins were buffer exchanged to remove guanidine hydrochloride with Amicon 3 kDa Centrifugal Filters. Samples were spun through the filter at 12,000 x *g* for 20 minutes and resuspended in 500 µL of 10 mM Tris-HCl (pH 7). This wash was spun down at 12,000 x *g* for 20 minutes, and the procedure was repeated 2 more times for a total of three washes with 10 mM Tris-HCl. The final addition of 10 mM Tris-HCl was spun as described above until the samples were reduced to 20 µL. Extracted proteins in 10 mM HCl were quantified using a bicinchoninic acid assay.

Proteolytic Digestion. For each individual bone sample, 20 µg of protein lysate was brought up to 4% SDS using a 10% SDS solution. Samples were then reduced using 20 mM dithiothreitol in 50 mM triethylammonium bicarbonate buffer (TEAB, pH 7) at 50 °C for 10 minutes, cooled to room temperature (RT) and held at RT for 10 minutes, and alkylated using 40 mM iodoacetamide in 50 mM TEAB (pH 7) at RT in the dark for 30 minutes. Samples were acidified with 12% phosphoric acid to obtain a final concentration of 1.2% phosphoric acid. S-Trap buffer (90% methanol in 100 mM TEAB at pH ~7.1) was added, and samples were loaded onto the S-Trap mini spin columns (Protifi, Farmingdale, NY). The entire sample volume was spun through the S-Trap mini spin columns at 4,000 x *g* at RT, binding the proteins to the mini spin columns. Subsequently, S-Trap mini spin columns were washed twice with S-Trap buffer at 4,000 x *g* at RT and placed into clean elution tubes. Samples were incubated for 1 hour at 47°C with sequencing grade trypsin (Promega, San Luis Obispo, CA) dissolved in 50 mM TEAB (pH 7) at a 1:25 (w:w) enzyme:protein ratio. Finally, additional trypsin solution was added at the same w:w ratio, and proteins were digested overnight at 37°C. Peptides were sequentially eluted from the mini S-Trap spin columns with 50 mM TEAB, 0.5% formic acid (FA) in water, and 50% acetonitrile (ACN) in 0.5% FA. After centrifugal evaporation, samples were resuspended in 0.2% FA in water and desalted with Oasis 10 mg Sorbent Cartridges (Waters, Milford, MA). The desalted elutions were subjected to centrifugal evaporation, and they were re-suspended in 0.2% FA in water at a final concentration of 1 µg/µL. Finally, indexed Retention Time Standards (iRT, Biognosys, Schlieren, Switzerland) were added to each sample, according to manufacturer's instructions (66).

Mass Spectrometric Analysis using Data-Independent Acquisition (DIA) and Data-Dependent Acquisition (DDA). Reverse-phase HPLC-MS/MS analyses were performed in DIA mode on a Dionex UltiMate 3000 system coupled online to an Orbitrap Eclipse Tribrid (Thermo Fisher Scientific, San Jose, CA). The solvent system consisted of 2% ACN, 0.1% FA in water (solvent A) and 98% ACN, 0.1% FA in water (solvent B). For the DIA acquisitions, digested peptides (200 ng) were loaded onto an Acclaim PepMap 100 C_{18} trap column (0.1 x 20 mm, 5-µm particle size; Thermo Fisher Scientific) over 5 minutes at 5 µL/minutes with 100% solvent A. Peptides were eluted on to an Acclaim PepMap 100 C_{18} analytical column (75 µm x 50 cm, 3-µm particle size;

Thermo Fisher Scientific) at 300 nL/minutes using the following gradient (indicated the % of solvent B): 2% B for 5 minutes, linear from 2% to 20% B in 95 minutes, linear from 20% to 32% B in 20 minutes, increase to 80% B in 1 minute, hold at 80% B for 9 minutes, and back to 2% B in 1 minute. The column was re-equilibrated for 29 minutes with 2% of solvent B/98% solvent A, and the total gradient length was 160 minutes. Each of the samples was acquired in DIA mode (47, 49, 50) in technical duplicates and in DDA mode. For DIA, survey MS1 spectra were collected at 120,000 resolution (Automatic Gain Control (AGC) target: 3e6 ions, maximum injection time: 60 ms, 350–1,650 *m/z*), and MS2 spectra at 30,000 resolution (AGC target: 3e6 ions, maximum injection time: Auto, Normalized Collision Energy: 27, fixed first mass 200 *m/z*). The DIA isolation scheme consisted of 26 variable windows covering the 350–1,650 *m/z* range with an overlap of 1 *m/z* per each window **(Supplemental Table S6)**. For the DDA acquisitions, digested peptides (200 ng) were loaded onto an Acclaim PepMap 100 C_{18} trap column (0.1 x 20 mm, 3-µm particle size; Thermo Fisher Scientific) over 10 minutes at 2 µL/minutes with 100% solvent A. Peptides were eluted on to an Acclaim PepMap 100 C_{18} analytical column (75 µm x 50 cm, 3-µm particle size; Thermo Fisher Scientific) at 300 nL/minutes using the following gradient (indicated the % of solvent B): 2% B for 10 minutes, linear from 2% to 20% B in 95 minutes, linear from 20% to 32% B in 20 minutes, increase to 80% B in 1 minute, hold at 80% B for 9 minutes, and back to 2% B in 1 minute. The column was re-equilibrated for 29 minutes with 2% of solvent B/98% solvent A, and the total gradient length was 165 minutes. For DDA, survey MS1 spectra were collected at 240,000 resolution (AGC target: 1.2e6 ions, maximum injection time: Auto, 350–1,500 m/z). Precursor ions with a charge state 2–5+ and an intensity above 2e4 were automatically selected for HCD fragmentation at NCE 27 in the orbitrap for a cycle time of 3 s. MS2 spectra were collected at 30,000 resolution (AGC target: 1e5 ions, maximum injection time: Auto, fixed first mass 200 *m/z*). Dynamic exclusion was set to 60 s.

Data-Independent Acquisition (DIA) Data Processing. DIA data files were processed in Spectronaut v16 (Biognosys) using directDIA. Data were searched against the *Mus musculus* reference proteome with 58,430 entries (UniProtKB-TrEMBL), accessed on 01/31/2018. Data extraction parameters were set as dynamic, and non-linear iRT calibration with precision iRT was

selected. Trypsin/P was set as the digestion enzyme, and two missed cleavages were allowed. Cysteine carbamidomethylation was set as a fixed modification, and methionine oxidation and protein N-terminus acetylation were set as dynamic modifications. For the protein level, identification was performed requiring a 1% q-value cutoff on the precursor ion and protein levels. Unique protein groups were reported with at least two unique peptide identifications. The protein level quantification was based on the peak areas of extracted ion chromatograms (XICs) of 3–6 MS2 fragment ions, specifically b- and y-ions, with local normalization and q-value sparse data filtering applied. In addition, iRT profiling was selected.

DDA Spectral Library Generation and DIA Quantification for Hydroxyproline-containing Peptide Level Analysis. A DDA spectral library was generated in Spectronaut v16 using slightly modified BGS settings and the same *Mus musculus* database. Briefly, for the Pulsar search, trypsin/P was set as the digestion enzyme and two missed cleavages were allowed. Cysteine carbamidomethylation was set as fixed modification, and proline oxidation, methionine oxidation, and protein N-terminus acetylation were set as variable modifications. Identifications were validated using 1% false discovery rate (FDR) at the peptide spectrum match (PSM), peptide and protein levels, and finally the best 3–6 fragments per peptide were kept. The spectral library contains 20,705 peptides and 2,372 protein groups, including 1,382 hydroxyproline-containing peptides corresponding to 85 hydroxyproline-containing protein groups (**Supplemental Table S7**). Identification was performed requiring a 1% q-value cutoff on the precursor ion and protein levels. The PTM site localization score was selected with a probability cutoff of 0.75. For PTM analysis, DIA data were processed in Spectronaut v16, using the generated DDA spectral library (described above). Quantification was based on XICs of 3 – 6 MS2 fragment ions, specifically b- and y-ions, without normalization and data filtering using q-value sparse. Grouping and quantitation of PTM peptides were accomplished using the following criteria: minor grouping by modified sequence and minor group quantity by mean precursor quantity.

Pathway Analysis. Over-representation analysis was performed using Consensus Path DB-mouse (Release MM11, 14.10.2021), developed by the bioinformatics group at the Max Planck Institute for Molecular Genetics (Berlin, Germany) (67, 68). The list of quantifiable proteins was used to

evaluate which gene ontology terms, including biological processes, molecular functions, and cellular components, were significantly enriched in these samples. Gene ontology terms identified from the over-representation analysis were subjected to the following filters: q-value < $1.0e^{-6}$, term category = b (biological processes), and term level ≥ 3. Dot plots were generated using the ggplot2 package (69) in R (version 4.0.5; RStudio, version 1.4.1106) to visualize significantly enriched biological processes from each comparison **(Supplemental Table S3)**.

Acknowledgement/Funding: We acknowledge the support from the National Institutes of Health NIH/NIA (U01 AG060906, PI: Schilling), Office of the Director for the Orbitrap Eclipse system (1S10 OD028654-01, PI: Schilling), NIDCR (R01 DE019284, PI: Alliston), The Glenn Foundation (Buck Institute, Patel), The Forever Healthy Initiative (PI: Schilling), T32 AG000266 to Schurman (PI: Campisi/Ellerby).

Associated Data: Raw data and complete MS data sets have been uploaded to the Center for Computational Mass Spectrometry, to the MassIVE repository at UCSD, and can be downloaded using the following link:

http://massive.ucsd.edu/ProteoSAFe/status.jsp?task=e01a701fe54e4fdd9f8f96b040395b99

(MassIVE ID number: MSV000090737; ProteomeXchange ID: PXD038207). [Note to the reviewers: To access the data repository MassIVE (UCSD) for MS data, please use: Username: MSV000090737_reviewer; Password: winter].

Figure Legends

Figure 1. Comparison of bone microenvironments in healthy and aged/diseased states. As bones age and the senescence burden increases, the bone microenvironment changes, which leads to bone fragility and degradation of cartilage. Additionally, osteocyte networks become less integrated, and chondrocytes become hypertrophic.

Figure 2. Sample workflow and strategy for Mass Spectrometry analysis. Femurs from wild-type mice were demineralized overnight using 1.2 M HCl and pulverized, and proteins were extracted for 72 hours at 4° C. The extracted protein lysates were digested and analyzed by MS in DIA mode for an in-depth proteome analysis.

Figure 3. Quality assessment of one bone sample workup injected in five technical replicates. Data acquisitions were assessed using A) precursor retention time regressions to illustrate acquisition to acquisition reproducibility and RT normalization, B) coefficient of variation (CV) vs abundance to determine precursor confidence, C) precursor %CV density to visualize precursor variability, and D) precursor CV distribution to quantify precursor reproducibility.

Figure 4. Proteomic results and Gene Ontology analysis for five wild-type femurs. Proteins identified in wild-type mouse femurs were analyzed using GO for both A) “cellular compartment” and B) “biological processes.” Sequence coverage for SPARC, an osteoblast marker, is highlighted in C) where green sections of the sequence are confidently identified in the proteomics. The spectrum analysis shown in D) displays the fragment ion series and fragment peaks for the peptide LEAGDHPVELLAR.

Figure 5. Overview of collagen subtypes identified in five wild-type mouse femurs. A bar graph showing the individual collagen genes confidently identified in the analysis and their respective quantities. Additionally, collagen structural families are quantified and denoted in A-F with their percent total represented in the bar graph.

Figure 6. Analysis of hydroxyproline modifications on collagen I alpha chain I. Two tryptic peptides of collagen 1 alpha chain 1 with highly-confident hydroxyproline site localizations due to specific and comprehensive fragmentation. A) Representative spectrum displaying the ion series for GDTGA**Pox**GA**Pox**GSQGA**Pox**GLQGM**Pox**GER. Fragmentation series provides site localization evidence to confirm modified prolines. B) Spectrum quantifying the intensity of precursor and fragment ions for the selected peptide. C) Similar representative spectrum displaying the near complete series of precursor and fragment ions for GLTGS**Pox**GSPGPDGK. D) Spectrum quantifying the intensity of precursor and fragment ions for the selected peptide.

Figure 7. Comparison of five wild-type mouse femurs to the core matrisome database and the Core SASP. A) Proteins identified from wild-type mouse femurs were compared to components of the core matrisome showing most representation of glycoproteins and ECM regulating proteins. B) Additional comparisons to the Core SASP show 131 overlapping identifications and only 19 unique core SASP proteins.

Supplemental Figure 1. Protein coverage for markers of major bone cell types with tryptic peptides in the sequence shown in green. Q05117: Tartrate-resistant acid phosphatase type 5 is a common marker to identify Osteoclasts showing a 42% peptide coverage. P07214: SPARC is a common marker to identify Osteoblasts showing a 51% peptide coverage. P70669: Phosphate-regulating neutral endopeptidase (PHEX) a common marker to identify Osteocytes showing a 39% peptide coverage.

References

1. Burr DB. Changes in Bone Matrix Properties with Aging. Bone. 2019;120:85-93.
2. Almeida M. Aging mechanisms in bone. Bonekey Reports. 2012;1(7).
3. Safiri S, Kolahi AA, Smith E, Hill C, Bettampadi D, Mansournia MA, et al. Global, regional and national burden of osteoarthritis 1990-2017: a systematic analysis of the Global Burden of Disease Study 2017. Ann Rheum Dis. 2020;79(6):819-28.
4. Gerosa L, Lombardi G. Bone-to-Brain: A Round Trip in the Adaptation to Mechanical Stimuli. Frontiers in Physiology. 2021;12.
5. Zhao Y, Suo Y, Yang Z, Hao Y, Li W, Su Y, et al. Inspiration for the prevention and treatment of neuropsychiatric disorders: New insight from the bone-brain-axis. Brain Research Bulletin. 2021;177:263-72.
6. Bajwa NM, Kesavan C, Mohan S. Long-term Consequences of Traumatic Brain Injury in Bone Metabolism. Front Neurol. 2018;9:115.
7. Kim HN, Chang J, Iyer S, Han L, Campisi J, Manolagas SC, et al. Elimination of senescent osteoclast progenitors has no effect on the age-associated loss of bone mass in mice. Aging Cell. 2019;18(3):e12923.
8. Alves RDAM, Demmers JAA, Bezstarosti K, van der Eerden BCJ, Verhaar JAN, Eijken M, et al. Unraveling the human bone microenvironment beyond the classical extracellular matrix proteins: a human bone protein library. Journal of Proteome Research. 2011;10(10):4725-33.
9. Demontiero O, Vidal C, Duque G. Aging and bone loss: new insights for the clinician. Ther Adv Musculoskelet Dis. 2012;4(2):61-76.
10. Tiede-Lewis LM, Xie Y, Hulbert MA, Campos R, Dallas MR, Dusevich V, et al. Degeneration of the osteocyte network in the C57BL/6 mouse model of aging. Aging (Albany NY). 2017;9(10):2190-208.
11. Schurman CA, Verbruggen SW, Alliston T. Disrupted Osteocyte Connectivity and Pericellular Fluid Flow in Bone with Aging and Defective TGF-β Signaling. Proc Natl Acad Sci USA. 2021;118(25):e2023999118.

12. Razi H, Birkhold AI, Weinkamer R, Duda GN, Willie BM, Checa S. Aging Leads to a Dysregulation in Mechanically Driven Bone Formation and Resorption. Journal of Bone and Mineral Research. 2015;30(10):1864-73.
13. Saita Y, Ishijima M, Kaneko K. Atypical femoral fractures and bisphosphonate use: current evidence and clinical implications. Therapeutic Advances in Chronic Disease. 2015;6(4):185 - 93.
14. Wainwright SA, Marshall LM, Ensrud KE, Cauley JA, Black DM, Hillier TA, et al. Hip Fracture in Women without Osteoporosis. J Clin Endocrinol Metab. 2005;90(5):2787 - 93.
15. Swain S, Coupland C, Mallen C, Kuo CF, Sarmanova A, Bierma-Zeinstra SMA, et al. Temporal Relationship between Osteoarthritis and Comorbidities: A Combined Case Control and Cohort Study in the UK Primary Care Setting. Rheumatology. 2021;60(9):4327-39.
16. Goldring MB, Goldring SR. Articular cartilage and subchondral bone in the pathogenesis of osteoarthritis. Ann N Y Acad Sci. 2010;1192(1):230 - 7.
17. Coppe JP, Desprez PY, Krtolica A, Campisi J. The senescence-associated secretory phenotype: the dark side of tumor suppression. Annu Rev Pathol. 2010;5:99-118.
18. Basisty N, Kale A, Jeon OH, Kuehnemann C, Payne T, Rao C, et al. A Proteomic Atlas of Senescence-Associated Secretomes for Aging Biomarker Development. Plos Biol. 2020;18(1):e3000599.
19. Coppe JP, Patil CK, Rodier F, Sun Y, Munoz DP, Goldstein J, et al. Senescence-associated secretory phenotypes reveal cell-nonautonomous functions of oncogenic RAS and the p53 tumor suppressor. Plos Biol. 2008;6(12):2853-68.
20. Hee JO, Nathaniel D, Judith C, H EJ. Senescent cells and osteoarthritis: a painful connection. Journal of Clinical Investigation. 2018;128(4):1229 - 37.
21. Freund A, Orjalo AV, Desprez PY, Campisi J. Inflammatory networks during cellular senescence: causes and consequences. Trends Mol Med. 2010;16(5):238-46.
22. Föger-Samwald U, Kerschan-Schindl K, Butylina M, Pietschmann P. Age Related Osteoporosis: Targeting Cellular Senescence. International Journal of Molecular Sciences. 2022;23(5):2701.
23. Pignolo RJ, Passos JF, Khosla S, Tchkonia T, Kirkland JL. Reducing Senescent Cell Burden in Aging and Disease. Trends Mol Med. 2020;26(7):630-8.

24. Peilin W, Songsong T, Chengyu Z, Zhi C, Chunhui M, Yinxian Y, et al. Directed elimination of senescent cells attenuates development of osteoarthritis by inhibition of c-IAP and XIAP. Biochimica Et Biophysica Acta Bba - Mol Basis Dis. 2019;1865(10):2618-32.

25. N FJ, G FD, Haitao W, Katharina J, B OM, M WM, et al. Identification of Senescent Cells in the Bone Microenvironment. Journal of Bone and Mineral Research. 2016;31(11):1920 - 9.

26. Kim H-N, Xiong J, MacLeod RS, Iyer S, Fujiwara Y, Cawley KM, et al. Osteocyte RANKL is required for cortical bone loss with age and is induced by senescence. Jci Insight. 2020;5(19):e138815.

27. Xiong J, Piemontese M, Onal M, Campbell J, Goellner JJ, Dusevich V, et al. Osteocytes, not Osteoblasts or Lining Cells, are the Main Source of the RANKL Required for Osteoclast Formation in Remodeling Bone. PLoS ONE. 2015;10(9):e0138189.

28. Wijenayaka AR, Kogawa M, Lim HP, Bonewald LF, Findlay DM, Atkins GJ. Sclerostin stimulates osteocyte support of osteoclast activity by a RANKL-dependent pathway. PloS one. 2011;6(10):e25900.

29. Farr JN, Xu M, Weivoda MM, Monroe DG, Fraser DG, Onken JL, et al. Targeting cellular senescence prevents age-related bone loss in mice. Nat Med. 2017;23(9):1072-9.

30. Ou Y, Zhou Y, Liang S, Wang Y. Sclerostin promotes human dental pulp cells senescence. Peerj. 2018;6:e5808.

31. Jeon OH, Kim C, Laberge RM, Demaria M, Rathod S, Vasserot AP, et al. Local clearance of senescent cells attenuates the development of post-traumatic osteoarthritis and creates a pro-regenerative environment. Nat Med. 2017;23(6):775-81.

32. Tabula Muris C. A single-cell transcriptomic atlas characterizes ageing tissues in the mouse. Nature. 2020;583(7817):590-5.

33. Yang C, Pang Y, Huang Y, Ye F, Chen X, Gao Y, et al. Single-cell transcriptomics identifies premature aging features of TERC-deficient mouse brain and bone marrow. Geroscience. 2022.

34. Boskey AL, Coleman R. Aging and bone. J Dent Res. 2010;89(12):1333-48.

35. Calciolari E, Donos N. Proteomic and Transcriptomic Approaches for Studying Bone Regeneration in Health and Systemically Compromised Conditions. PROTEOMICS – Clinical Applications. 2020;14(3):1900084.

36. Hynek R, Michalus I, Cejnar P, Šantrůček J, Seidlová S, Kučková Š, et al. In-bone protein digestion followed by LC-MS/MS peptide analysis as a new way towards the routine proteomic characterization of human maxillary and mandibular bone tissue in oral surgery. ELECTROPHORESIS. 2021;42(23):2552-62.

37. Tsolis KC, Bei ES, Papathanasiou I, Kostopoulou F, Gkretsi V, Kalantzaki K, et al. Comparative proteomic analysis of hypertrophic chondrocytes in osteoarthritis. Clinical Proteomics. 2015;12(1):12.

38. Zhang H, Recker R, Lee W-NP, Xiao GG. Proteomics in bone research. Expert review of proteomics. 2010;7(1):103-11.

39. Nielson CM, Jacobs JM, Orwoll ES. Proteomic studies of bone and skeletal health outcomes. Bone. 2019;126:18-26.

40. Bonicelli A, Di Nunzio A, Di Nunzio C, Procopio N. Insights into the Differential Preservation of Bone Proteomes in Inhumed and Entombed Cadavers from Italian Forensic Caseworks. J Proteome Res. 2022;21(5):1285-98.

41. Bell PA, Solis N, Kizhakkedathu JN, Matthew I, Overall CM. Proteomic and N-Terminomic TAILS Analyses of Human Alveolar Bone Proteins: Improved Protein Extraction Methodology and LysargiNase Digestion Strategies Increase Proteome Coverage and Missing Protein Identification. Journal of Proteome Research. 2019;18(12):4167-79.

42. Hudson DM, Eyre DR. Collagen prolyl 3-hydroxylation: a major role for a minor post-translational modification? Connect Tissue Res. 2013;54(4-5):245-51.

43. Marini JC, Forlino A, Cabral WA, Barnes AM, San Antonio JD, Milgrom S, et al. Consortium for osteogenesis imperfecta mutations in the helical domain of type I collagen: regions rich in lethal mutations align with collagen binding sites for integrins and proteoglycans. Hum Mutat. 2007;28(3):209-21.

44. Besio R, Chow CW, Tonelli F, Marini JC, Forlino A. Bone biology: insights from osteogenesis imperfecta and related rare fragility syndromes. FEBS J. 2019;286(15):3033-56.

45. Jiang X, Ye M, Jiang X, Liu G, Feng S, Cui L, et al. Method Development of Efficient Protein Extraction in Bone Tissue for Proteome Analysis. Journal of Proteome Research. 2007;6(6):2287-94.

46. Rose J, Basisty N, Zee T, Wehrfritz C, Bose N, Desprez PY, et al. Comprehensive proteomic quantification of bladder stone progression in a cystinuric mouse model using data-independent acquisitions. PLoS One. 2022;17(6):e0250137.

47. Gillet LC, Navarro P, Tate S, Röst H, Selevsek N, Reiter L, et al. Targeted data extraction of the MS/MS spectra generated by data-independent acquisition: a new concept for consistent and accurate proteome analysis. Mol Cell Proteomics. 2012;11(6):O111.016717-O111.

48. Schilling B, Gibson BW, Hunter CL. Generation of High-Quality SWATH((R)) Acquisition Data for Label-free Quantitative Proteomics Studies Using TripleTOF((R)) Mass Spectrometers. Methods Mol Biol. 2017;1550:223-33.

49. Collins BC, Hunter CL, Liu Y, Schilling B, Rosenberger G, Bader SL, et al. Multi-laboratory assessment of reproducibility, qualitative and quantitative performance of SWATH-mass spectrometry. Nat Commun. 2017;8(1):291-.

50. Bruderer R, Bernhardt OM, Gandhi T, Xuan Y, Sondermann J, Schmidt M, et al. Optimization of Experimental Parameters in Data-Independent Mass Spectrometry Significantly Increases Depth and Reproducibility of Results. Mol Cell Proteomics. 2017;16(12):2296-309.

51. Bekker-Jensen DB, Bernhardt OM, Hogrebe A, Martinez-Val A, Verbeke L, Gandhi T, et al. Rapid and site-specific deep phosphoproteome profiling by data-independent acquisition without the need for spectral libraries. Nat Commun. 2020;11(1):787.

52. Muntel J, Gandhi T, Verbeke L, Bernhardt OM, Treiber T, Bruderer R, et al. Surpassing 10 000 identified and quantified proteins in a single run by optimizing current LC-MS instrumentation and data analysis strategy. Mol Omics. 2019;15(5):348-60.

53. Young MF, Kerr JM, Ibaraki K, Heegaard AM, Robey PG. Structure, expression, and regulation of the major noncollagenous matrix proteins of bone. Clin Orthop Relat Res. 1992(281):275-94.

54. Shoulders MD, Raines RT. Collagen structure and stability. Annu Rev Biochem. 2009;78:929-58.

55. Ricard-Blum S. The collagen family. Cold Spring Harb Perspect Biol. 2011;3(1):a004978.

56. Olsen BR. Chapter 10 - Matrix Molecules and Their Ligands. In: Lanza R, Langer R, Vacanti J, editors. Principles of Tissue Engineering (Fourth Edition). Boston: Academic Press; 2014. p. 189-208.

57. Doll S, Burlingame AL. Mass spectrometry-based detection and assignment of protein posttranslational modifications. ACS Chem Biol. 2015;10(1):63-71.

58. Pokidysheva E, Zientek KD, Ishikawa Y, Mizuno K, Vranka JA, Montgomery NT, et al. Posttranslational modifications in type I collagen from different tissues extracted from wild type and prolyl 3-hydroxylase 1 null mice. J Biol Chem. 2013;288(34):24742-52.

59. Naba A, Clauser KR, Ding H, Whittaker CA, Carr SA, Hynes RO. The extracellular matrix: Tools and insights for the "omics" era. Matrix Biol. 2016;49:10-24.

60. Naba A, Clauser KR, Hoersch S, Liu H, Carr SA, Hynes RO. The matrisome: in silico definition and in vivo characterization by proteomics of normal and tumor extracellular matrices. Mol Cell Proteomics. 2012;11(4):M111 014647.

61. Naba A, Pearce OMT, Del Rosario A, Ma D, Ding H, Rajeeve V, et al. Characterization of the Extracellular Matrix of Normal and Diseased Tissues Using Proteomics. J Proteome Res. 2017;16(8):3083-91.

62. Gonzalez-Garcia C, Cantini M, Ballester-Beltran J, Altankov G, Salmeron-Sanchez M. The strength of the protein-material interaction determines cell fate. Acta Biomater. 2018;77:74-84.

63. De Belly H, Paluch EK, Chalut KJ. Interplay between mechanics and signalling in regulating cell fate. Nat Rev Mol Cell Biol. 2022;23(7):465-80.

64. Northey JJ, Weaver VM. Mechanosensitive Steroid Hormone Signaling and Cell Fate. Endocrinology. 2022;163(8).

65. Creecy A, Brown KL, Rose KL, Voziyan P, Nyman JS. Post-translational modifications in collagen type I of bone in a mouse model of aging. Bone. 2021;143:115763.

66. Escher C, Reiter L, MacLean B, Ossola R, Herzog F, Chilton J, et al. Using iRT, a normalized retention time for more targeted measurement of peptides. Proteomics. 2012;12(8):1111-21.

67. Kamburov A, Pentchev K, Galicka H, Wierling C, Lehrach H, Herwig R. ConsensusPathDB: toward a more complete picture of cell biology. Nucleic Acids Research. 2011;39(suppl_1):D712-D7.

68. Kamburov A, Wierling C, Lehrach H, Herwig R. ConsensusPathDB—a database for integrating human functional interaction networks. Nucleic Acids Research. 2009;37(suppl_1):D623-D8.

69. Wickham H. ggplot2: Elegant Graphics for Data Analysis: Springer-Verlag New York; 2016.

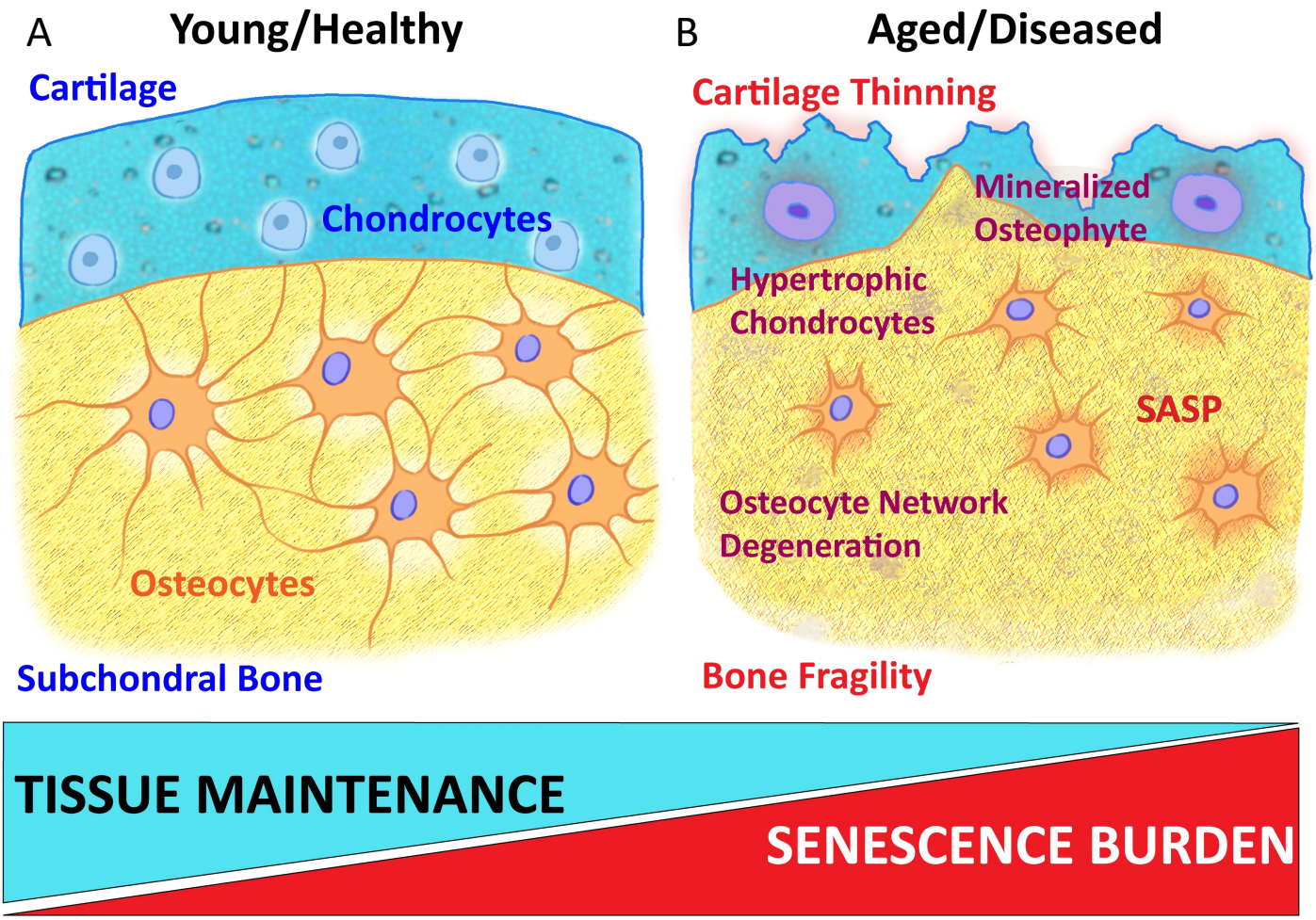
A
Young/Healthy
Cartilage
Chondrocytes
Osteocytes
Subchondral Bone
B
Aged/Diseased
Cartilage Thinning
Mineralized
Osteophyte
Hypertrophic
Chondrocytes
SASP
Osteocyte Network
Degeneration
Bone Fragility
TISSUE MAINTENANCE
SENESCENCE BURDEN

Figure 1

Bone Protein Extraction from a complex matrix

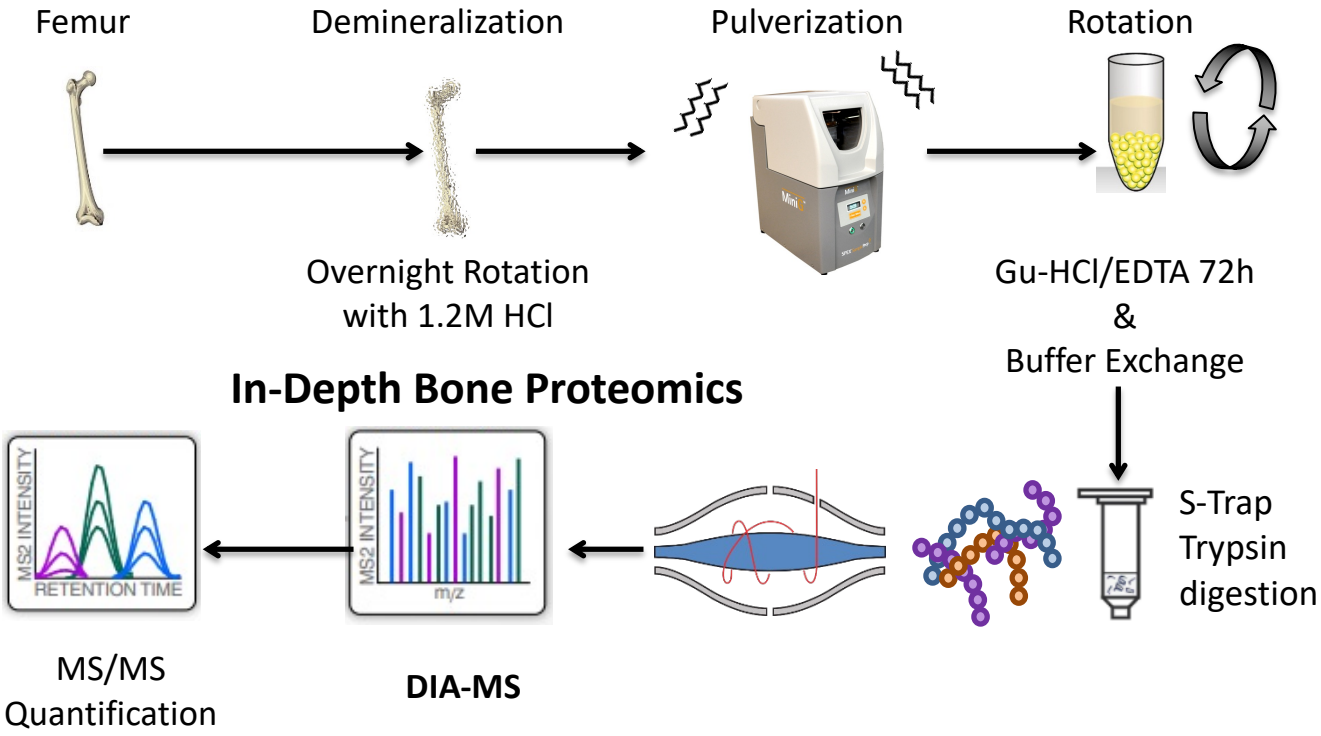

Figure 2

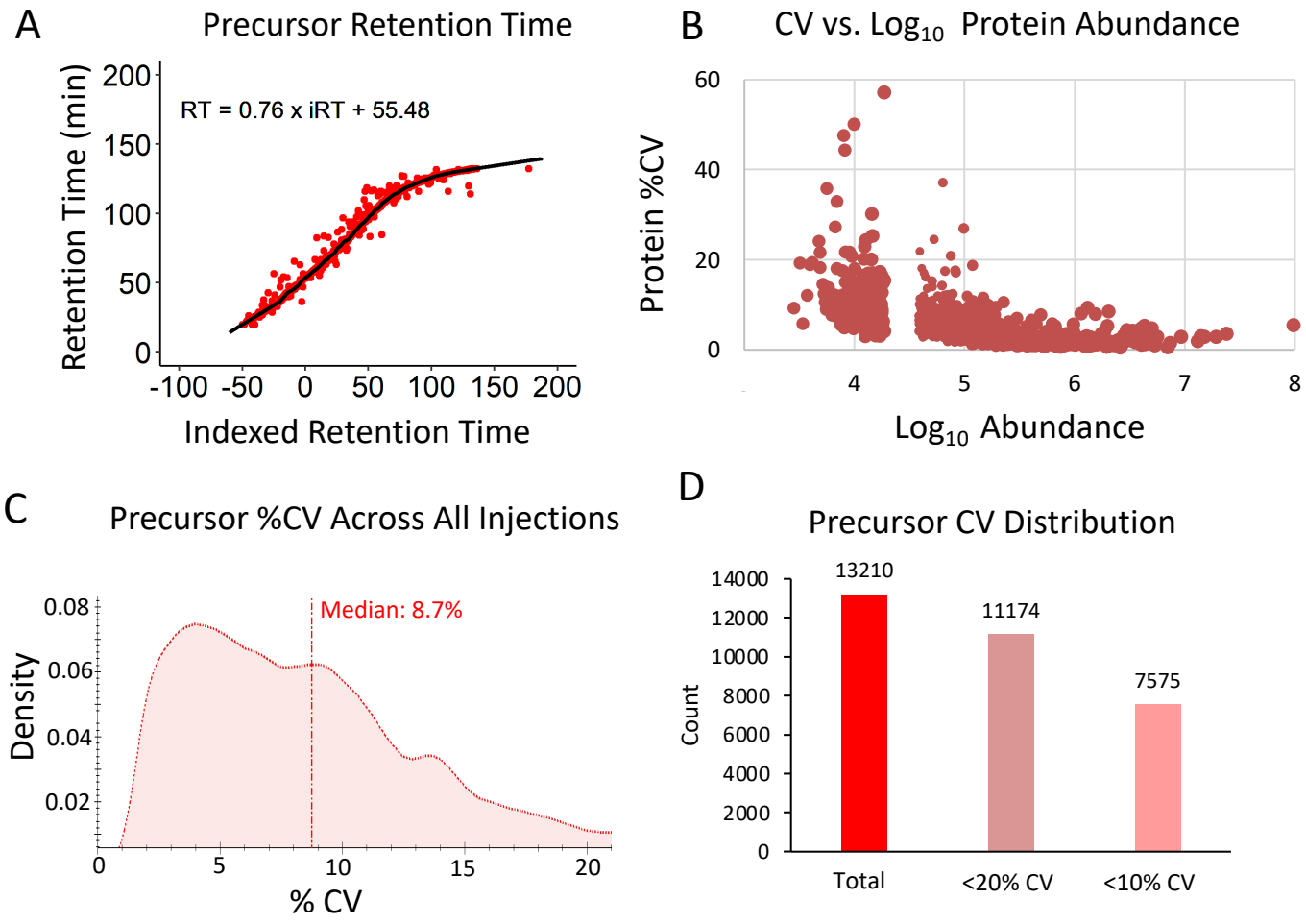
A
Precursor Retention Time
RT = 0.76 x iRT + 55.48
Retention Time (min)
Indexed Retention Time
B
CV vs. Log10 Protein Abundance
Protein %CV
Log10 Abundance
C
Precursor %CV Across All Injections
Median: 8.7%
Density
% CV
D
Precursor CV Distribution
13210
11174
7575
Count
Total
<20% CV
<10% CV

Figure 3

A Cellular Compartment

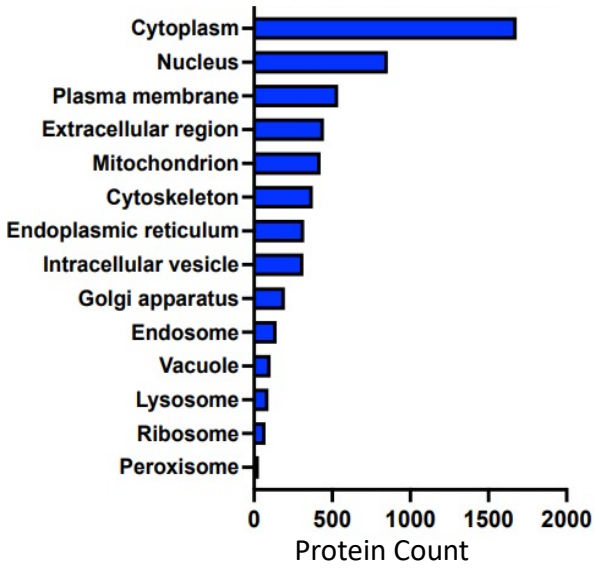

B Biological Processes

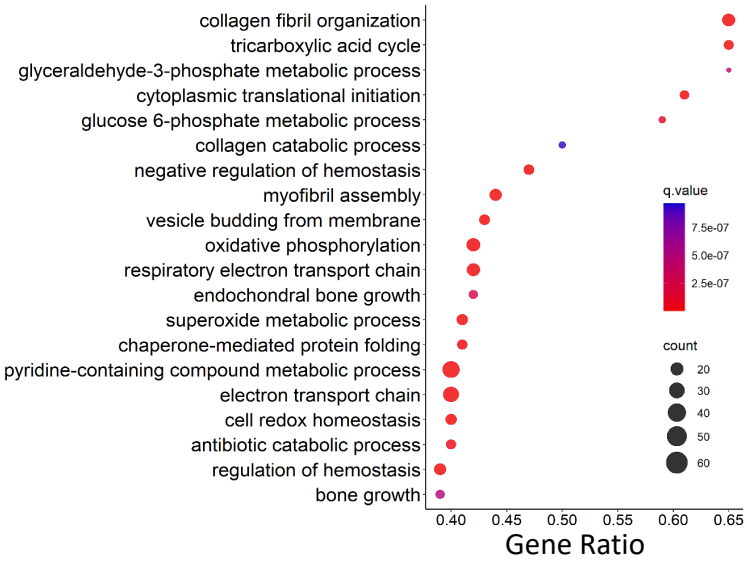

C Osteoblast Marker

P07214 SPARC: 51% Protein Coverage

MRAWIFFLLCLAGRALAAPQQTEVAEEIVEEETVVEETGVPVGANPVQVEMGEFEDGAEETVEEVVADNPCQNHHCKH
GKVCELDESNTPMCVCQDPTSCPAPIGEFEKVCSNDNKTFDSSCHFFATKCTLEGTKKGHKLHLDYIGPCKYIAPCLDSELT
EFPLRMRDWLKNVLVTLYERDEGNNLLTEKQKLRVKKIHENEKRLEAGDHPVELLARDFEKNYNMYIFPVHWQFGQLDQ
HPIDGYLSHTELAPLRAPLIPMEHCTTR FFETCDLDNDK YIALEEWAGCFGIK EQDINKDLVI

D SPARC

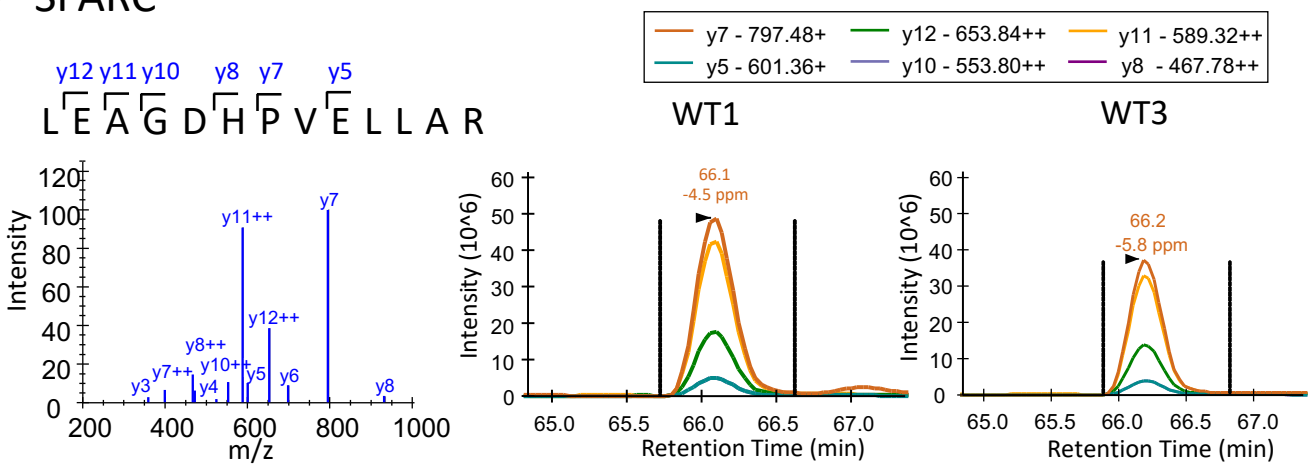

Figure 4

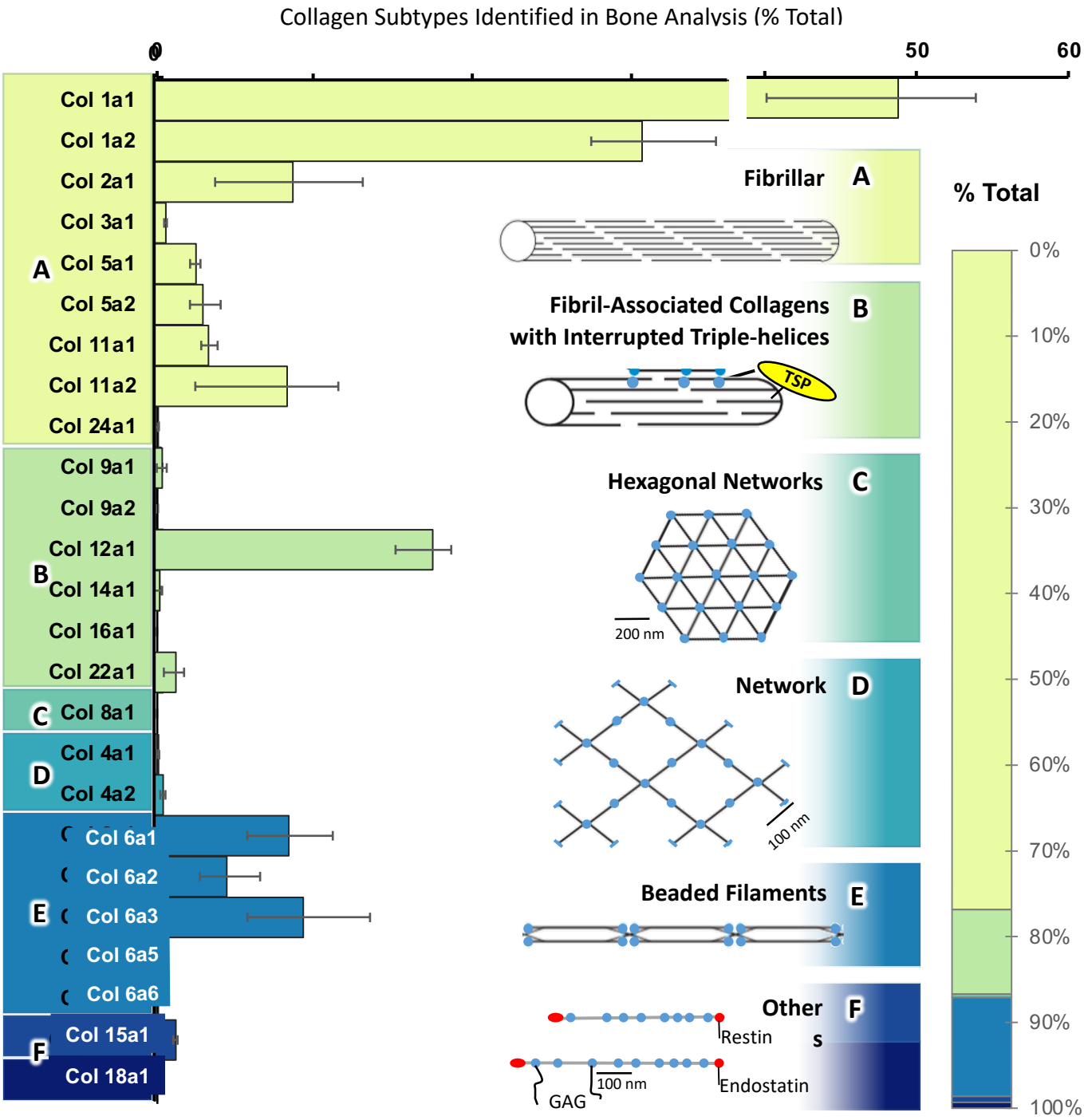
Collagen Subtypes Identified in Bone Analysis (% Total)
0
50
60
Col 1a1
Col 1a2
Col 2a1
Col 3a1
A
Col 5a1
Col 5a2
Col 11a1
Col 11a2
Col 24a1
Col 9a1
Col 9a2
Col 12a1
B
Col 14a1
Col 16a1
Col 22a1
C
Col 8a1
Col 4a1
D
Col 4a2
Col 6a1
Col 6a2
E
Col 6a3
Col 6a5
Col 6a6
Col 15a1
F
Col 18a1
Fibrillar
A
Fibril-Associated Collagens
with Interrupted Triple-helices
B
TSP
Hexagonal Networks
C
200 nm
Network
D
100 nm
Beaded Filaments
E
Other
s
F
Restin
100 nm
GAG
Endostatin
% Total
0%
10%
20%
30%
40%
50%
60%
70%
80%
90%
100%

Figure 5

A

Collagen type I alpha I chain

Figure 6

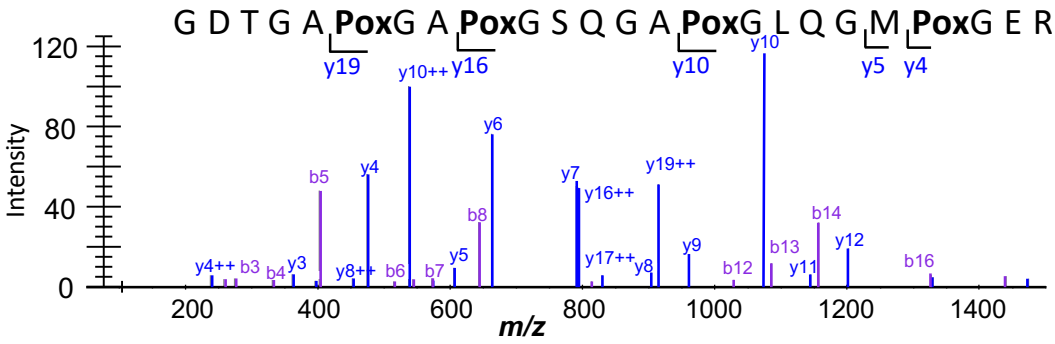

B

GDTGA**Pox**GA**Pox**GSQGA**Pox**GLQGM**Pox**GER

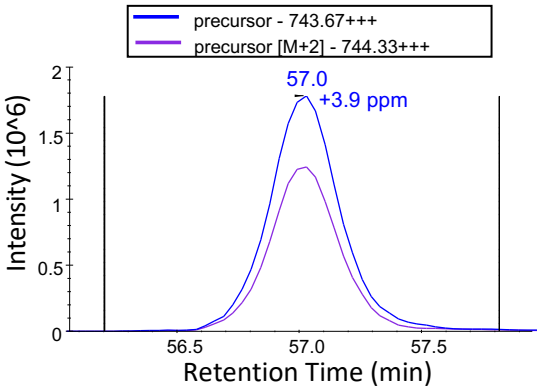

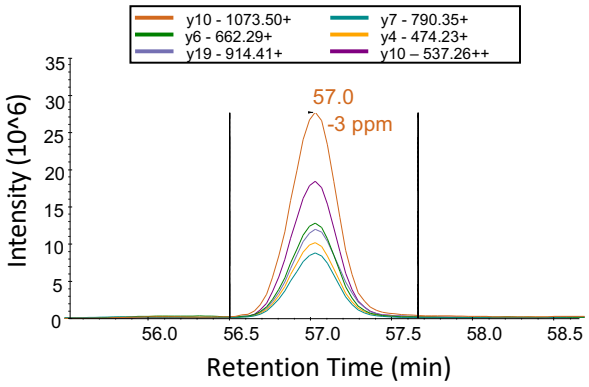

C

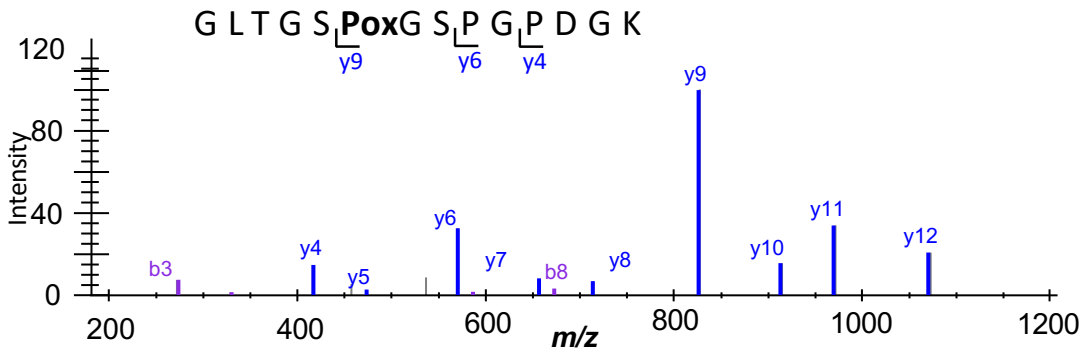

D

GLTGS**Pox**GSPGPDGK

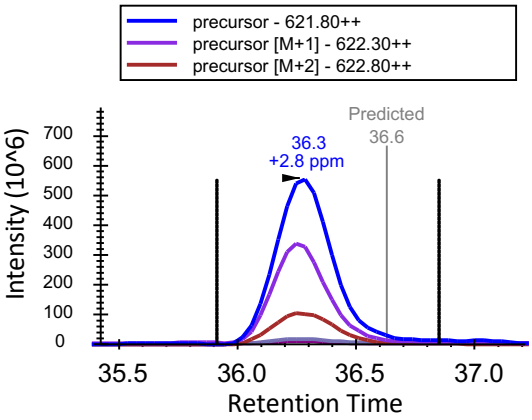

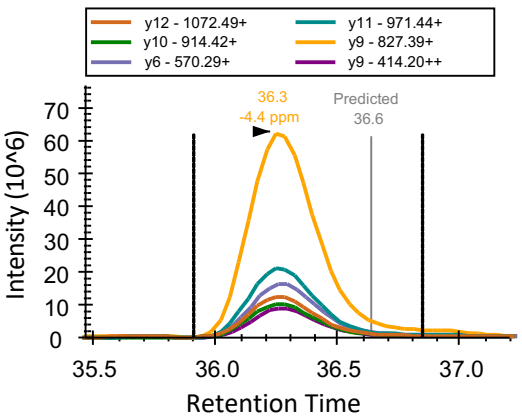

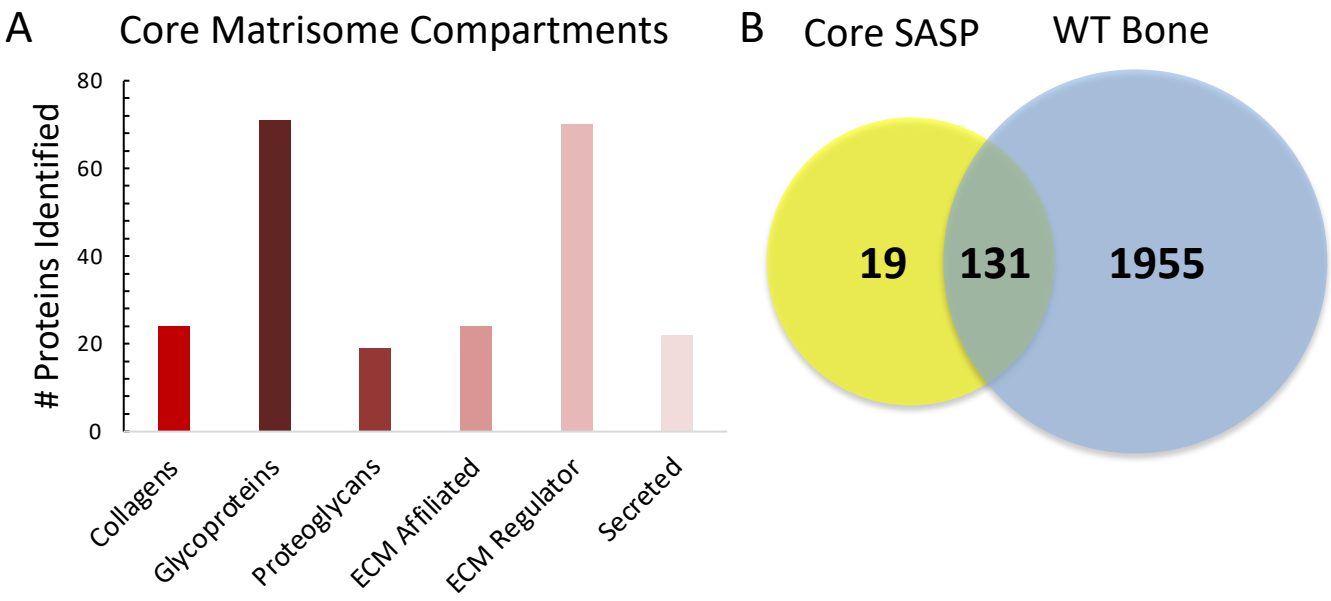
A
Core Matrisome Compartments
Proteins Identified
80
60
40
20
0
Collagens
Glycoproteins
Proteoglycans
ECM Affiliated
ECM Regulator
Secreted
B
Core SASP
WT Bone
19
131
1955

Figure 7